Heliyon 6 (2020) e05384

Contents lists available at ScienceDirect

Heliyon

journal homepage: www.cell.com/heliyon

Research article

Synthesis of thermal insulator using chicken feather fibre in starch-clay nanocomposites

Rasheed Babalola [a], Augustine O. Ayeni [b,*], Peter S. Joshua [a], Ayodeji A. Ayoola [b], Ukeme O. Isaac [c], Umo Aniediong [a], Vincent E. Efeovbokhan [b], James A. Omoleye [b]

[a] Akwa Ibom State University, College of Engineering, Department of Chemical/Petrochemical Engineering, Akpaden, Mpat Enin, Nigeria
[b] Covenant University, College of Engineering, Department of Chemical Engineering, Canaan Land, Ota, Nigeria
[c] Federal Polytechnic Oko, College of Engineering, Department of Chemical Engineering, Oko, Anambra State, Nigeria

ARTICLE INFO

Keywords:
Chemical engineering
Materials science
Nanotechnology
Nanomaterials
Materials application
Materials processing
Materials synthesis
Thermal insulator
Nanofiller
Chicken feather
Nanocomposite
Crystallographic

ABSTRACT

Incorporating chicken feather fibre (CFF) into natural based-nanocomposite comprising of glycerine plasticized-cassava starch binder with bentonite (BNT) as nanofiller, a thermal insulator (TIN) was synthesized. Central Composite Design (CCD) Response Surface Methodology was employed to carry out the experimental design using two factors (CFF and BNT) along with one response (thermal conductivity) to produce nine materials as insulators, comprising of 0%, 5%, and 10% BNT based on 8 g initial weight of CFF. A sample without CFF was used as the control. Developed thermal insulators were subjected to thermal conductivity tests using Lee's disc method at a steady state. The best insulator is TIN-4 with the lowest thermal conductivity of 0.0313 W/(mK) and the highest insulation property of 114.63 m^2k/W, while TIN-10 with no CFF has the highest thermal conductivity of 0.0549 W/(mk) and lowest insulation property of 48.1603 m^2k/W. Proportionate use of chicken feather fibre in starch-clay nanocomposite will help synthesize an effective thermal insulator with minimum cost.

1. Introduction

The improper management or disposal of by-products of materials processed from industrial, domestic, social, and commercial activities has posed many problems to the ecosystem. Effective waste management is expensive [1]. Global production of the chicken feather as waste is estimated to be about 15 million tons per year [1]. The burning of this waste brings about the release of harmful substances into the air [1, 2].

Production of thermal insulators using chicken feathers will address the challenge of waste disposal and create wealth from waste. Materials of low thermal conductivity are known as thermal insulators; they are used to reduce heat transfer between material in contact. The thermal conductivities of some materials, as reported somewhere [1, 3, 4] confirmed that chicken feather fibre (CFF) has very low thermal conductivity with unique structures and properties compare to any other natural or synthetic fibre [5, 6]. This justifies its use for thermal insulator and ease of wide industrial application. For instance, low-density value (0.8 g/cm^3 compared to about 1.5 g/cm^3 and 1.3 g/cm^3 for cellulose fiber and wool, respectively), excellent compressibility and resiliency, ability to dampen sound, and distinctive morphological structures [6, 7, 8] make them unique. Chicken feathers contain about 91% keratin protein, 1% lipids, and 8% water [9] comprising of three different parts, the rachis, the barbs, and the barbules, which are attached one to the other (the barbules to the barbs and the barbs to the rachis) [10].

Feathers are in two microcrystalline forms, the fiber, and the quill. The thermal energy required to perturb the quill is less than that required by fibers; hence, the fibres can withstand thermal and mechanical stress [5]. The elasticity moduli of feather keratin range from 0.045 GPa to 10 GPa, while the tensile strength of oven-dried CFF, in the range of 41–130 MP (5). Thermogravimetric analysis of CFF, as reported elsewhere [11] suggests that the drying temperature for this fiber should be above 328.15K, with the processing temperature of a reinforced composite being controlled below 493.15K. Differential scanning calorimetry of CFF indicated that temperatures below 383.15K may not allow for moisture progression [12]. The utilization of chicken feather barbs for use as a thermal insulator relates to its intriguing property of honeycomb structure and thermal resistivity ability due to air pockets in the feather [13, 14]. The binding of chicken feathers in

* Corresponding author.
E-mail addresses: augustine.ayeni@covenantuniversity.edu.ng, aoayeni@gmail.com (A.O. Ayeni).

https://doi.org/10.1016/j.heliyon.2020.e05384
Received 10 June 2020; Received in revised form 15 July 2020; Accepted 27 October 2020

various composites has been achieved by using various polymers such as chitosan-starch blend, high-density polyethylene (HDPE), elastic polyurethane, polylactic acid, polybutyrate adipate terephthalate, and polyvinyl alcohol [4, 15, 16, 17, 18, 19].

This study considered the use of glycerine-plasticized cassava starch (CST) as a binder. Starch has been used for composites production in various works [20, 21, 22, 23]. According to Van Heemst *et al.* [24], cassava starch occurs naturally as a granular structure and cannot be used directly as a thermoplastic material except by destructuring through mechanical works at elevated temperatures in the presence of water and other possible processing agents e.g. plasticisers like polyols and fatty acids, forming thermoplastic starch (TPS) [25]. The end products of starch have poor dimensional stability and mechanical properties [26, 27, 28]. Still, its limitations can be resolved by introducing plasticizers (such as glycerine, glycol, and sorbitol) to enhance flexibility and processing ability [29, 30, 31]. TPS and nanocomposite mixture possess improved thermal and mechanical properties [32, 33, 34, 35].

Nanomaterials'shape and size have widespread applications in industries and research fields such as their introduction into polymer matrix [36]. Their usage as doped material has improved the properties of the polymer [37, 38, 39]. Nanofillers are introduced in the polymer at rates from 1-10% by mass. The composites' properties are impacted by organic matrix and nanofiller mixture ratio [40] to yield improved mechanical, thermal, and fire retardation [41, 42]. The most widely used clay-based nanocomposites are the smectites (such as montmorillonite, bentonite and hectorite) [43]. Montmorillonites have a high cation exchange capacity, which is little affected by particle size. Therefore, the cation exchange capacity allows both inorganic and organic cations to bind [44], maximizing its utilization as a nanofiller to improve the composition's properties.

In this study, novel thermal insulators (TIN) were produced by incorporating CFF into glycerine plasticized-cassava starch (CST) and bentonite (BNT) nanocomposite. This study seeks the thermal insulators' production such that naturally available materials (BNT was used as doped nanofiller and strength impacts while CST was used as a binder) to convert waste chicken feathers to thermal insulators. Furthermore, this study was to develop insulators which are not dependent on synthetic polymers, thereby minimizing some health and ecosystem related issues instigated by synthetic polymers and the after use of chicken feather waste. Performance evaluation was carried out using the Lee's disc method of thermal conductivity test. The proposed CFF in starch-clay nanocomposites synthesis of TIN is convenient, economical, and environmentally friendly, thereby encouraging the conversion of waste to wealth.

2. Materials and method

2.1. Materials, reagent, and equipment

The chicken feathers were sourced in form of wastes from a poultry farm in Eket Village, Eket Local Government Area, Akwa Ibom State, Nigeria. Cassava tubers were obtained from the farm in Etinan Local Government Area, Akwa Ibom State, Nigeria. Industrial bentonite, glycerine, and 98% ethanol were obtained from Ekpo Scientific Enterprises, Eket Local Government Area, Akwa Ibom State, Nigeria. Equipment and apparatus used include mechanical sieving machine with 0.2 mm mesh size sieve, ceramic mortar and pestle, Soxhlet extractor, heating mantle, hot plate, electronic weighing balance, 500 ml beakers, 50 ml measuring cylinder, thermometer, inextensible string, steam can, micrometer screw guage, vernier caliper, Lee's disc apparatus, stainless steel batch reactor, manual compression pressing machine, electronic oven and universal testing machine.

2.2. Preparation of chicken feather fibre powder

The first step of the preparation process was cleaning chicken feathers by washing with soap and water. The feathers were utterly cleaned and then dried in a convection oven at 318.15 K for seven days to ensure complete evaporation. Fibre was then separated from the quill through scissors, and the feathers were grounded using mortar and pestle. Lipids present in the ground feathers were removed by contacting 20 ml of ethanol with 8 g of the feather powder, using Soxhlet extractor for 4 h. The lipid-free feather particles obtained were then dried and stored at room temperature.

2.3. Production of starch from cassava

The cassava roots obtained from the farm were peeled. The peeled roots were washed and grated. Small volumes of water were added to the grated cassava and stirred vigorously. The slurry obtained was filtered in a sieve of mesh size 140 μm. The filtrate was allowed to settle for 2 h and the supernatant decanted. The starch mash was dried in an oven until a moisture content of 10%–15% was obtained. The starch obtained was milled and packed at room temperature.

2.4. Production of feather/starch-clay nanocomposite

The design of experiments was achieved using the response surface methodology technique (central composite design (CCD)) with the aid of Design Expert 11 software (Table 1). Two factors (CFF and BNT) were used as the independent variables to obtain the dependent variable or the response, thermal conductivity. The effect of 0 g CFF content (i.e. TIN-10) was considered as the control. The starch was kept constant while varying the weight of BNT and CFF. The composites were produced considering 0%, 5%, and 10% BNT (nanofillers were introduced in the polymer at rates from 1–10% by mass) [40] to 8 g initial weight of CFF. At 0% concentration of BNT based on 8 g initial CFF, the CFF concentration is 8 g (100%); 5% BNT based on 8 g initial weight of CFF produced 0.40 g BNT with 7.6 g CFF; and 10% BNT based on 8 g initial weight of CFF produced 0.80 g BNT with 7.2 g CFF.

The experimental runs (Table 1) were generated with the CCD response surface methodology with the two factors (A = CFF and B = BNT) considered using their lowest weight content (A = 7.2 g and B = 0 g) and the highest weight content (A = 8 g and B = 0.80 g) selected based on the percentages considered above. The ten experimental runs were carried out with a constant composition of 20 g of starch, 35 ml of water and 6 ml of glycerol. The raw materials were feed into the reactor and mixed in this order; CST, water, glycerol, and CFF.

The reaction proceeded with continuous stirring for about 30 min, at 373.15K. The rigid material obtained was transferred to a cylindrical mold, compressed in a cylindrical mold, and cooled to 298.15k. The resulting composites were oven-dried at 100 °C and kept for further studies.

2.5. Analytical method

2.5.1. Dimensional analysis

The average thickness, d (mm), of the samples was measured with a micrometer screw gauge by measuring five different points on the material [45]. The diameter, D (mm) of the samples obtained as well (using the same approach as in thickness) through the use of an electronic digital caliper (ISO9001).

2.5.2. X-ray diffraction (XRD) analysis

XRD analysis was used to check for the nanofiller properties utilized to ascertain whether the material is BNT as desired. The XRD analysis

Table 1. The experimental design generated using central composite design.

Run	1	2	3	4	5	6	7	8	9	10
Factor1 (A: CFF)	8.16	8	7.6	7.6	8	7.04	7.6	7.2	7.2	0
Factor 2 (B: BNT)	0.4	0.8	0.97	0.4	0	0.4	0	0	0.8	0.4

was operated with the continuous scan type from 5° 2θ to 75° 2θ diffractometer with step time of 32.90 s, the temperature of 298.15K, and generator settings kept at 40 mA and 45 kV. Copper anode (λ = 1.54060 Å) material was used to carry out this analysis.

2.5.3. Thermal conductivity test

The thermal conductivity test was achieved using Lee's disc experiment (Figure 1). Through a steam can, steam was generated and allowed to pass over the nano-sized composite material produced with its outlet connected to the steam chamber's inlet using a rubber tube. In the meantime, the weight of the Lee's disc, M, was obtained with a weighing balance. The specific heat capacity of the metal slab, C was recorded from a constant table. The composite was placed on metal slab (the disc) and then the steam chamber on the composite and suspended from the clamp stand. A thermometer was inserted into the Lee's disc and the steam chamber, allowed to read until a constant temperature was obtained for these thermometers. Steady-state temperatures were attained and recorded as T_1 and T_2 for the steam chamber and disc, respectively. Constant temperature reading by the thermometers was recorded after 10 min. The thermometers were interchanged, and the new temperatures at steady state were recorded, then the average of the readings was recorded ($T_{MC}$and T_{MA} for disc and chamber, respectively). The steam chamber was raised, and the composite was removed. The steam chamber directly heated Lee's disc until its temperature was about T_{MC}+ 283.15K in steady-state (Figure 1). The steam chamber was removed with the heat allowed to distribute uniformly for 2–3 min over the disc. The composite material was then placed on the disc while observing the temperature reading of the thermometer. With the disc allowed to cool to T_{MC}, the temperature was read and recorded immediately for every 30 s (using a stopwatch) until the temperature falls to about 283.15K below the temperature, T_{MC}.. Using Microsoft Excel 2007, the rate of cooling, $\frac{\partial T}{\partial t}$ for each composite was deduced. Conductive heat flow occurs in the decreasing temperature (from the steam chamber through the sample to the disc). Fourier's Law expresses conductive heat transfer, as shown in Eq. (1).

$$H = \kappa \frac{\pi D^2 (T_{MC} - T_{MA})}{4d} \tag{1}$$

At steady state, the mean temperatures, T_{MC} and T_{MA} are constant, and the rate of heat transfer (H) through the disc equal heat loss (Equation 2), using the cooling rate of the top brass disc covered with the chicken feather insulation, the cooling rate ($\frac{dT}{dt}$) was determined.

$$H = MC\frac{dT}{dt} \tag{2}$$

Combining Eqs. (1) and (2), the thermal conductivity, κ, was obtained as given in Eq. (3). Where M is the mass of the lower disc, and C is the specific heat.

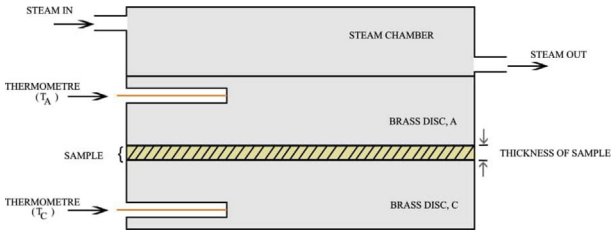

Figure 1. Schematic diagram of the Lee's disc experiment.

$$\kappa = \frac{4MC\left(\frac{dT}{dt}\right)d}{\pi D^2 (T_{MC} - T_{MA})} \tag{3}$$

2.5.4. Comparison of the experimental with the predicted values

The experimental response values obtained were tested for accuracy by comparing the experimental values with the predicted values of the CCD generated model. Design Expert 11.1.2.0 was used for the design and interpretation of results. The significance of the quadratic model was also tested with analysis of variance (ANOVA).

3. Results and discussion

3.1. Sample diameter measurement

The average diameter, D, and thickness, d of the thermal insulator (TIN) samples (TIN-1 to TIN-10) were measured and recorded as given in Table 2. The insulators (Figure 3(a)) with CFF were seen to have more thickness than the sample without the CFF (TIN-10) in it.

3.2. XRD analysis

The XRD analysis of BNT nanofiller is as provided in Figure 2. The diffractogram showed that the substance contains two minerals: montmorillonite and gypsum, and both minerals have a monoclinic crystal system. The chemical formula for the montmorillonite (MMT) is $Si_{7.80}Al_{1.72}Cs_{0.16}Fe_{0.20}Mg_{0.28}O_{20.00}$, while for gypsum is $Ca_{4.00}S_{4.00}O_{24.00}H_{4.00}$. The crystallographic parameters are given in Table 3. Bentonite is an aluminuimphyllosillicate clay generated frequently from the alteration of volcanic ash consisting mostly of smectite minerals, usually montmorillonite [46].

In addition to montmorillonite, it contains a small portion of other mineral matter like quartz, zeolites, gypsum, pyrite, or feldspar [47]. From Figure 2, the pattern shows that the substance contains MMT which is the major mineral formed at various peaks which can be seen at 7.10 2θ with the d-spacing of 12.4369Å, 26.512 2θ (d = 3.3459Å), 29.12 2θ (d = 3.0665Å), 36.63 2θ (d = 2.4531Å), 61.93 2θ (d = 1.44984Å) and further reflection at 68.06 2θ (d = 1.3777Å). Also, gypsum was noticed at about 11.66 2θ with a d-spacing of 7.5869Å and further confirmed at 23.63 2θ with a d-spacing of 3.7653Å. The diffractogram generated is similar to works carried out by Carlson, 2004 [48] and El Miz *et al.*, 2017 [49].

3.3. Thermal conductivity analysis

The mass M of the Lee's disc was measured and recorded as 0.7794 kg, while the specific heat capacity of brass, C, was obtained as 0.38 kJ/kg K [50]. The mean temperature at steady state (Table 4) was obtained from the experimental setup, Figure 3(b).

The influence of the CFF can be noticed (Table 4) on the temperature readings. Sample TIN-10 having no CFF allowed more heat to pass through it. For the mean temperature of 370.45K recorded by the thermometer inserted into A (the steam chamber), the sample allowed more heat to pass through it with 341.15K temperature of the disc. The higher the ability of a sample to retain heat, the lesser the heat released to C. This means, the higher the conductivity of heat by the insulator, the higher the temperature value read by the thermometer. Better retention of heat was observed by the insulators, TIN-1 to TIN-9 (with CFF) instead of TIN-10 with no CFF. The temperature recorded by TIN-1 to TIN-9 was

Table 2. Average thickness, d, and diameter, D, of the insulators.

Sample	d (mm)	D (mm)
TIN-1	3.300	100.322
TIN-2	3.516	97.032
TIN-3	2.888	101.480
TIN-4	2.848	101.346
TIN-5	3.246	108.312
TIN-6	3.588	106.686
TIN-7	3.520	106.532
TIN-8	3.430	99.094
TIN-9	3.378	102.194
TIN-10	2.644	95.524

Table 3. Crystallographic parameters of the minerals in the BNT.

Crystallographic Parameters	Mineral	
	Montmorillonite	Gypsum
a (Å)[a]	5.181	6.2742
b (Å)	8.945	5.67
c (Å)	12.34	5.67
Alpha (Å)	90	90
Beta (Å)	99.62	113.908
Gamma (Å)	90	90
Calculated density (g/cm^3)	1.84	2.27

[a] Å (Angstrom unit) = 10^{-10}m.

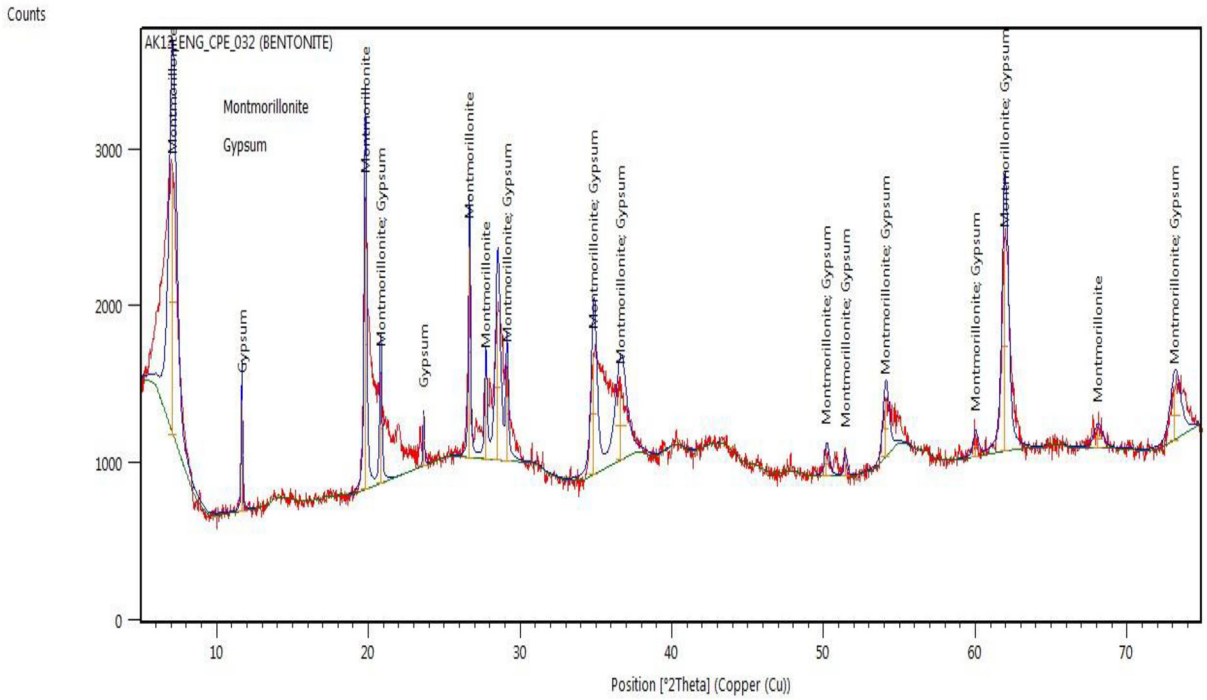

Figure 2. X-Ray diffractogram for the BNT nanofiller.

much lesser than that of TIN-10 (Table 4). This result shows the tendency of CFF to retard heat flow.

The synthesized TIN's insulation efficiency was determined by measuring the cooling rate of the brass disc at steady-state temperature with the brass disc top covered with synthesized TIN. The disc's temperature in each run was recorded per minute and represented in Figure 4, and their respective coefficient of determination R^2 was recorded in Table 5. The linearity of temperature with time was observed from the temperature per time plot that temperature reduces with increasing time (Figure 4 and Table 5).

At steady-state, the rate of cooling is the same as the rate of heating. Hence, the rate of cooling $\left(\frac{dT}{dt}\right)$ was obtained (Figure 4), where the cooling temperature for each of the experimental run was measured per 30 s after the steady-state temperature was attained and recorded in Table 4. The plot for each of the samples has a negative slope (Figure 4), indicating the drop in temperature due to cooling experienced by the disc through heat loss to the environment and the covering insulator. The cooling rate ($\frac{dT}{dt}$) for sample TIN-1 to TIN-10 are given in Table 5. The cooling rate in each case is almost similar, with the highest value observed to be 0.023 K/s in TIN-5 and the lowest being 0.013 K/s in TIN-2, accounting for only a difference of 0.10 K/s between the highest and lowest rate. The coefficient of determination R^2 was used to assess the experimental data's accuracy or fitness (Table 5). From Table 5, the obtained R squared values were above 97%, indicating accuracy since they are close to 100%. The values obtained for the parameters needed to achieve the thermal conductivity (κ) for each of the samples were substituted into Eq. (3). Table 5 shows relevant parameters for the different insulators.

3.3.1. *Comparison of the thermal conductivity of the samples based on the weight of BNT*

The thermal conductivity across the thermal insulators as given in Table 5, was further evaluated categorically based on their BNT weight concentrations. Four groups, namely; 0 g, 0.4 g, 0.8 g, and 0.97 g, were considered. TIN-5, TIN-7, and TIN-8 fall under 0 g BNT; TIN-1, TIN-6, and TIN-10 fall under 0.4g BNT; TIN-2 and TIN-9 fall under 0.8g BNT; and finally, TIN-3 (being the only sample) falls under 0.97g BNT.

Considering the 0 g BNT group, the samples' thermal conductivity increased with a reduction in CFF content from samples TIN-5, TIN-7 to TIN-8. The thermal conductivity values across each sample were deduced as 0.0520 W/(mK), 0.0571 W/(mK), and 0.0593 W/(mK),

Table 4. Mean steady-state temperature for the insulators.

Sample		TIN-1	TIN-2	TIN-3	TIN-4	TIN-5	TIN-6	TIN-7	TIN-8	TIN-9	TIN-10
T_M (K)	TMA	369.75	369.75	367.15	369.45	367.65	369.65	364.45	368.45	369.65	370.45
	TMC	320.15	317.15	317.05	315.45	322.45	316.65	327.65	319.65	324.05	341.15

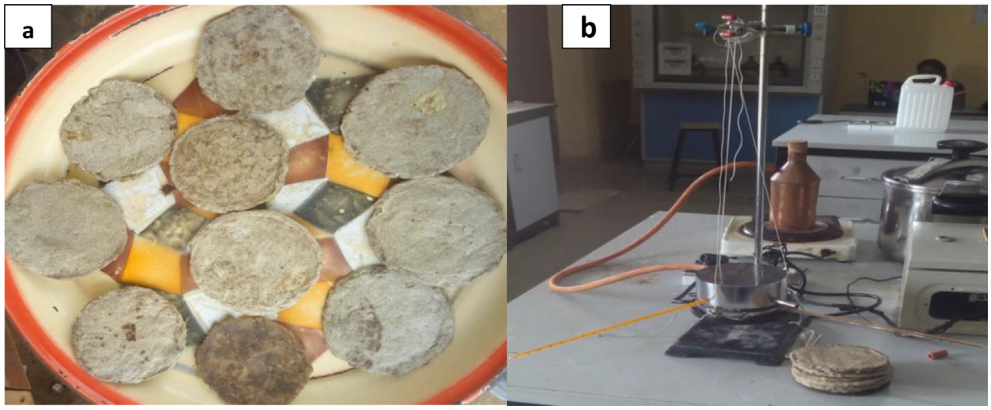

Figure 3. (a) The developed insulator and (b) The experimental set up of Lee's method for the thermal conductivity test.

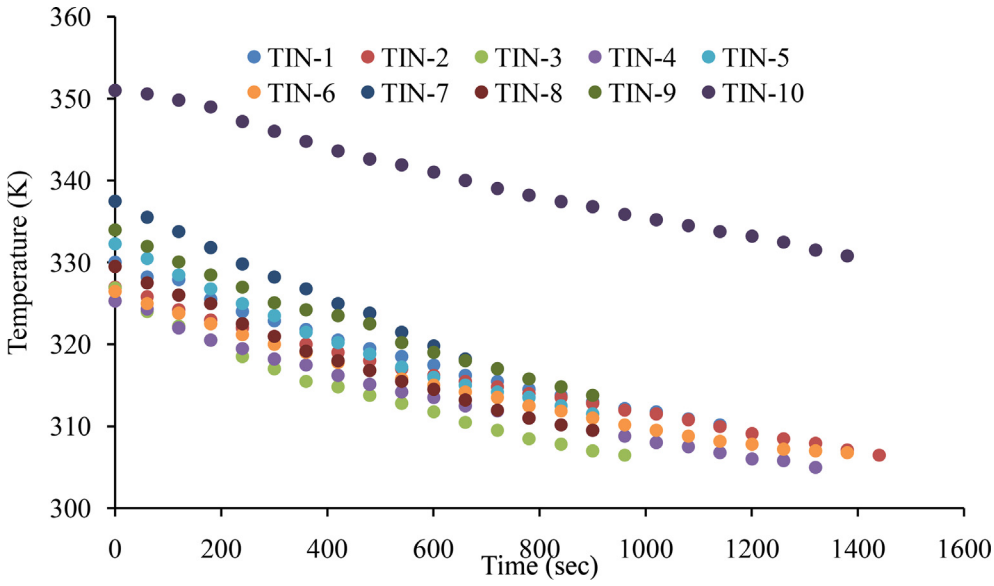

Figure 4. Variation in temperature of the synthesized TIN with time.

Table 5. Parameters and their values for the thermal insulators.

Sample	BNT (g)	(K/s)	R^2	'κ' W/(mK)	R_T (mK/W)	R_V (m^2K/W)
TIN-1	0.4	0.017	0.982	0.038	26.385	87.071
TIN-2	0.8	0.013	0.999	0.035	28.736	101.035
TIN-3	0.97	0.02	0.970	0.042	23.697	68.436
TIN-4	0.4	0.014	0.977	0.031	31.949	90.990
TIN-5	0.0	0.023	0.981	0.052	19.231	62.423
TIN-6	0.4	0.014	0.977	0.032	30.960	111.084
TIN-7	0.0	0.018	0.998	0.057	17.513	61.646
TIN-8	0.0	0.022	0.986	0.059	16.863	57.842
TIN-9	0.8	0.021	0.991	0.056	17.825	60.214
TIN-10	0.4	0.014	0.990	0.055	18.215	48.160

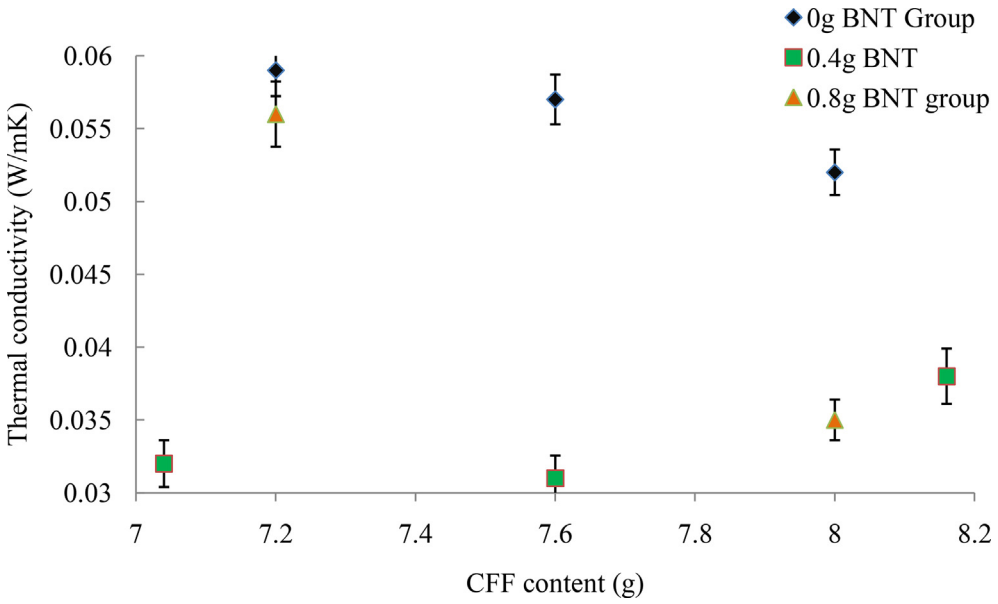

Figure 5. Categorical comparison of samples based on BNT content.

respectively (Figure 5). Thermal conductivities for the 0.4g BNT category were 0.0379 W/(mk), 0.0313 W/(mK), 0.0323 W/(mK), and 0.0549 W/(mK) for TIN-1, TIN-4, TIN-6, and TIN-10 respectively. The 0.4 g BNT followed the similar trend as that of 0 g BNT with the only exception for TIN-1 with a greater κ value than TIN-4 which could be due to the environmental condition at which the experiment was conducted. For the 0.8 g BNT group, TIN-2 and TIN-9 made up of 8 g, and 7.2 g of CFF have κ value 0.0348 W/(mK) and 0.0561 W/(mK) respectively. The thermal conductivity for TIN-2 is lesser than that of TIN- 9 (Figure 5). Finally, the 0.97 g BNT with TIN-3 the thermal conductivity value of 0.0422 W/(mK).

The effect of CFF on the thermal conductivity (Figure 6) is that increase in CFF content resulted in decreased thermal conductivity, indicating that CFF has suitable insulation property. Since the property of a thermal insulator is also obtained as thermal resistivity, R_T (the inverse of thermal conductivity), the higher the resistivity, the better the insulation property of the material.

Comparing best insulators in these groups, for the group 0 g BNT, TIN-8 is the best insulator with a 0.0593 W/mK thermal conductivity. The 0.4g BNT group has TIN-4 with 0.0313 W/(mK) as the best. TIN-2 with thermal conductivity of 0.0348 W/(mK) for 0.8 g BNT group. Finally, TIN-3 of 0.97 g BNT (the only sample if this group) has 0.0422 W/(mK).

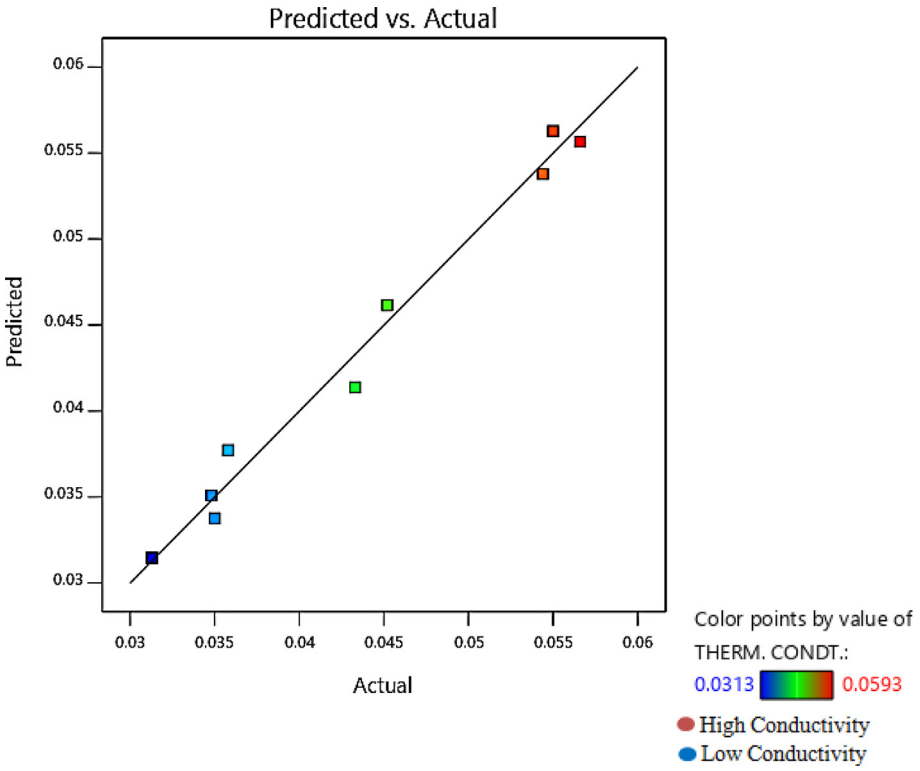

Figure 6. The plot of predicted (W/mK) against actual value (W/mK) for the response.

Table 6. Diagnostics reports showing Experimental, Actual, Predicted and Residual Values for adjustment.

Sample		TIN-1	TIN-2	TIN-3	TIN-4	TIN-5	TIN-6	TIN-7	TIN-8	TIN-9	TIN-10
Response (Therm. Cond.)	Experimental	0.0379	0.0348	0.0422	0.0313	0.052	0.0323	0.0571	0.0593	0.0561	0.0549
	Value										
	Actual Value	0.035	0.0348	0.0452	0.0313	0.055	0.0358	0.0544	0.0566	0.0433	-
	Predicted Value	0.0338	0.0351	0.0461	0.0315	0.0563	0.0377	0.0538	0.0557	0.0414	-
Residual (experimental – predicted value)		0.0012	-0.0003	-0.0009	-0.0002	-0.0013	-0.0019	0.0006	0.0009	0.0019	-
Leverage		0.64	0.626	0.664	0.462	0.734	0.64	0.413	0.734	0.626	-
Internally Studentized Residuals		1.16	-0.262	-0.913	-0.118	-1.376	-1.781	0.449	1.019	1.756	-
Externally Studentized Residuals		1.234	-0.229	-0.888	-0.102	-1.641	-3.392	0.399	1.025	3.177	-
Cook's Distance		0.399	0.019	0.274	0.002	0.87	0.941	0.024	0.477	0.858	
Influence on Fitted Value DFFITS		1.646	-0.296	-1.249	-0.095	-2.726	-4.524	0.335	1.702	4.107	
Standard Order		6	4	8	9	2	5	7	1	3	

Table 7. Fit statistics of the R^2.

Std. Dev.	0.0018	R^2	0.9859
Mean	0.0423	Adjusted R^2	0.9683
C.V. %	4.25	Predicted R^2	0.8773
		Adequate Precision	17.8542

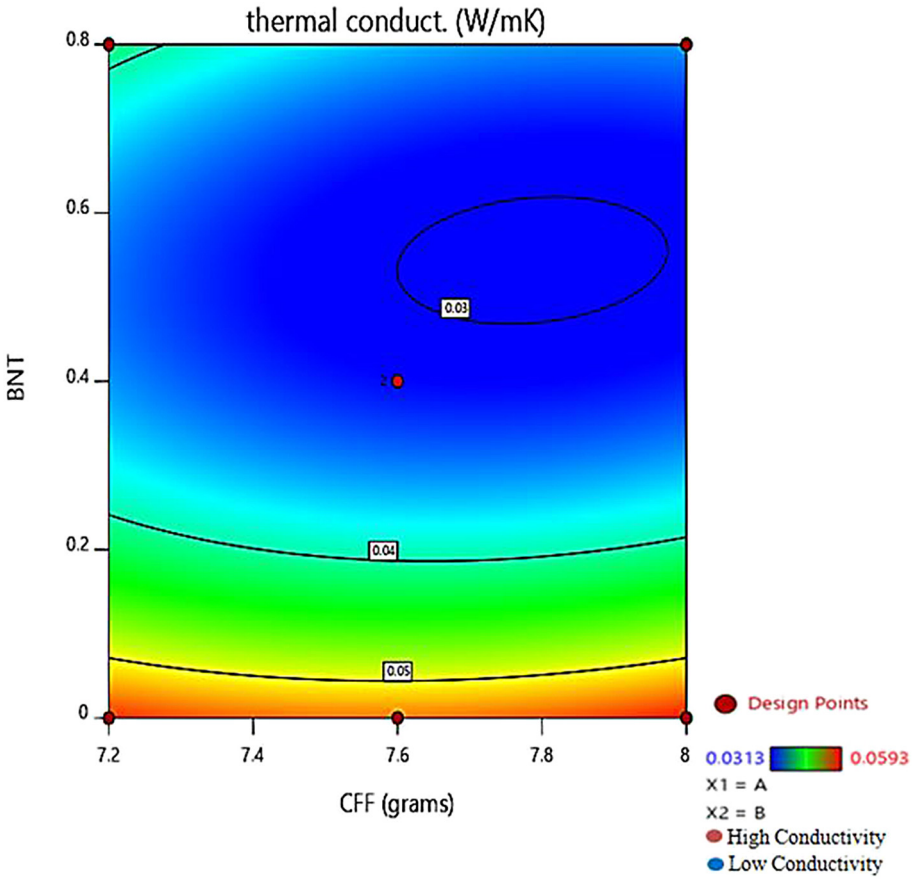

Figure 7. The contour plot of predicted (thermal conductivity) against BNT and CFF.

Considering these insulators, TIN-4 with 0.0313 W/(mK) has the lowest heat flow allowance, accounting for the best property as an insulator. TIN-10 with 0 g CFF has a thermal conductivity of 0.0549 W/(mK), which is the highest in the 0.4 g BNT group. TIN-10 can be termed as having the most deficient insulation property with no CFF compared to the rest materials in this group. The results are similar to that reported elsewhere [4, 52].

3.3.2. *The resistance value (R_V)*

The resistance value (Table 5) is a property for checking how well a material resists conductive flow [51, 52]. The higher the R_V, the more excellent its resistance and so its thermal insulating property. The 0% containing CFF nanocomposite was the least of this property (48.1603 m^2K/W) than the other insulators. The highest value was noticed for TIN-6 (111.0836 m^2K/W), followed by TIN-2 with 101.0345 m^2K/W,

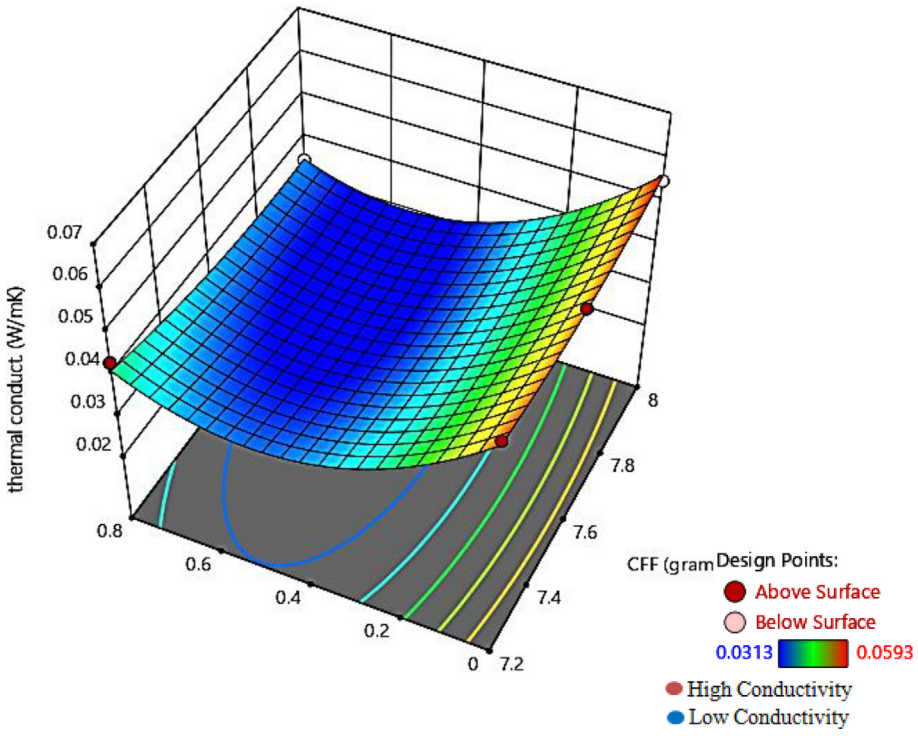

Figure 8. 3D Surface response of thermal conductivity versus CFF and BNT.

Table 8. ANOVA (analysis of variance) of quadratic model.

Source	Sum of Squares	DOF	Mean Square (Variance)	F-value	p-value	Interpretation
Model	0.0009	5	0.0002	56.05	0.0009	Highly significant
A-CFF	0.0000	1	0.0000	4.94	0.0904	Marginally significant
B-BNT	0.0005	1	0.0005	156.03	0.0002	Highly significant
AB	0.0000	1	0.0000	3.70	0.1269	Not significant
A^2	0.0000	1	0.0000	7.12	0.0559	Significant
B^2	0.0006	1	0.0006	191.55	0.0002	Highly significant
Residual	0.0000	4	3.22E-06			
Lack of Fit	0.0000	3	4.29E-06			
Pure Error	0.0000	1	0.0000			
Cor Total	0.0009	9				

and TIN-4 with 90.9904 m^2K/W. Others are TIN-1, TIN-3, TIN-5, TIN-7, TIN-8, and TIN-9 following sequentially. However, it is often preferred for economic reasons that a thermal insulator should offer excellent resistance to heat flow at a lower thickness. Considering this fact, TIN-4 with a lesser thickness of 2.84 m is preferable, compared to TIN-6 (3.588 m) and TIN-2 (3.516 m). If we assume that TIN-4, TIN-6, and TIN-2 were all made up of 3.588 m thickness (as possessed by TIN-6 with the highest R-value), then TIN-4 will maintain even a higher R_V of 114.6326 m^2K/W TIN-6 and TIN-2 with R_V of 111.0836 m^2K/W and 103.1034 m^2K/W.

3.4. Comparison of experimental and the predicted values from CCD

The experimental results obtained were compared to the predicted values by the CCD method, where the R^2 was obtained as 0.8773. To get an R^2 above 0.8999, the response (thermal conductivity) attained were adjusted (Tables 6 and 7) to fit with the response predicted. The fit statistics is presented in Table 7. The predicted R^2 of 0.8773 is in reasonable agreement with the adjusted R^2 of 0.9683 because of the difference of which is less than 0.2 (Design Expert 11). Also, adequate precision, which measures the signal to noise ratio (where a ratio greater than 4 is desirable) was found to be a ratio of 17.854. This indicated that the signal was adequate. Therefore, this model (Equation 4) can be used to navigate the design space. The lack of fit and degrees of freedom analysis was obtained as 3, which agrees with the recommended value of at least three and pure error of one. These conditions ensured a valid lack of fit test.

$$K = 0.0315 - 0.0014A - 0.0089B - 0.0017AB + 0.0022A^2 + 0.0135B^2 \quad (4)$$

The plot of predicted against the actual value of the response (thermal conductivity) is given in Figure 6 shows a close agreement of the actual values with the predicted value. The contour (Figure 7) shows a value of 0.03W/(mK), which is almost similar to the experimental value of 0.0313W/(mK) (sample 4). The interaction between BNT and CFF on the thermal conductivity response is presented in Figure 8. The contour plot and the 3D response curves help analyze the interactions between factors on the responses, determining optimum levels for factors and responses [53, 54]. In the diagnostic report (Table 7), the leverage for each run is reported with values greater than 0 and less than 1. The leverage of a point ranges from 0 to 1 and indicates how much an individual design point influences the model's predicted values. The more the leverage is closer to 1, the more the residual value will be closer to 0. Hence, the

closeness of the observed values of the experiment to the predicted values can be noticed from the table.

3.5. Analysis of variance

Analysis of variance (ANOVA), as provided in Table 8, was applied to the results to determine the statistical significance and fitting of the quadratic model to this study. From the fit summary where different process orders were examined like the linear model, quadratic, cubic, mean, linear, and the interactions were tested, the quadratic was seen to have the highest F-value and lowest P-value. Hence, the quadratic model was selected for the analysis. The quadratic model was further tested to obtain more statistical results. The model fitness test is achieved by checking for F-test. When a *P*-value for a test is less than 5%, it implies that a model term is significant. The F-test returned an F-value of 56.05 and p-value (<0.05), which implies that the model adopted for the study is accurate and highly significant. The amount which the model prediction missed the observation known as lack of fit under the degrees of freedom (DOF) analysis column (Table 8) was obtained as 3, which is in agreement with the recommended value of at least three (3). This conditioned, along with a pure error of 1 ensured a valid lack of fit test. The terms expressed in model for B (linear value), A^2 and B^2 (squared values) are significant model terms. Meaning that the linear effect of BNT (B) and the quadratic effects of A (CFF) and B (BNT) are significant in the production of the insulator. P-value > 0.10 indicates the model terms are not significant, and this is the case with term AB (interaction of CFF and BNT on production of insulator is not significant, having no pronounced effect).

4. Conclusion

In this study, thermal insulators were developed using CFF in composite with BNT as nanofiller and starch binder. Nanocomposites of 0%, 5% and 10% bentonite clay to 8 g of feather were formed. The quadratic process model was analyzed using ANOVA. The thermal conductivity (κ) of the composites materials is affected by the BNT content of the samples and was noticed by the various categories. Better insulation property was observed by group 0.4 g BNT in TIN-4 with 0.0313 W/mk against 0 g BNT in TIN-8 with 0.0593 W/mk, 0.8 g BNT in TIN-2 with 0.0348 W/mk and 0.9 g BNT in TIN-3 with κ of 0.0422 W/mk. However, the control sample TIN-10 with 0 g of CFF has the highest κ value of 0.0549 W/mk and can be termed the poorest in terms of thermal conductivity and with the least insulation property of 48.1603 m^2k/W. In contrast, sample TIN-4 has the highest value of 114.63 m^2k/W. The experimental value thus agreed with the predicted values obtained from the central composite design through leverage analysis.

5. Recommendation

This study seeks the development and encouragement of synthetic-independent thermal insulators where waste chicken feathers are used as the primary source by curtailing some health and ecosystem related issues instigated by synthetic polymers and the after use of chicken feather waste. Hence, it is recommended that:

i. More investigations should be carried out on the application of chicken feather wastes to develop synthetic-independent thermal insulators, which will be an inexpensive raw material for the industry.
ii. Thermogravimetry and thermal diffusivity studies should be carried out to better diversify and harness the application of the CFF as a thermal insulator.
iii. Utilization of this material as an alternative thermal insulation source whose application will be useful in construction, domestic and industrial purposes due to its light weight and low cost.

Declarations

Author contribution statement

Rasheed Babalola: Conceived and designed the experiments; Performed the experiments; Analyzed and interpreted the data; Wrote the paper.

Augustine O. Ayeni: Analyzed and interpreted the data; Contributed reagents, materials, analysis tools or data; Wrote the paper.

Peter S. Joshua: Performed the experiments; Analyzed and interpreted the data.

Ayodeji A. Ayoola & Vincent E. Efeovbokhan: Analyzed and interpreted the data; Contributed reagents, materials, analysis tools or data.

Ukeme O. Isaac: Analyzed and interpreted the data.

Umo Aniediong: Performed the experiments; Analyzed and interpreted the data; Wrote the paper.

James A. Omoleye: Contributed reagents, materials, analysis tools or data.

Funding statement

This research did not receive any specific grant from funding agencies in the public, commercial, or not-for-profit sectors.

Competing interest statement

The authors declare no conflict of interest.

Additional information

No additional information is available for this paper.

Acknowledgements

The authors appreciate the Management of Akwa Ibom State University for providing the enabling environment for this study and Covenant University, Canaan land, Ota, Nigeria, for sponsoring the publication of this study.

References

[1] Worldbank, Solid Waste Management. Understanding Poverty Urban Development, April, 2019. http://www.worldbank.org/en/topic/urbandevelopment/brief/solid-waste-management.
[2] J.J. Van Heemst, E. Zant, G.G.J. Schennink, J. Rodenburg, T. Rodenburg, Starch-based Biodegradable Polymer; Method of Manufacture and Articles Thereof, Patent EP2493975B1(2010), 4th April, 2019. https://patents.google.com/patent/EP249397B1#similarDocuments.
[3] W. Ye, M.R. Broughton, Chicken feather as a fibre source for nonwoven insulation, Int. Nonwovens J. 8 (2019) 1–9.
[4] X. Qin, Chicken Feather Fibre Mat/PLA Composites for thermal Insulation, Master of Engineering Thesis, The University of Waikato, 2015, https://researchcommons.waikato.ac.nz/bitstream/handle/10289/9371/thesis.pdf?sequence=3&isAllowed=y.
[5] S.K. Chinta, S.M. Landage, K. Yadav, Application of chicken feathers in technical textiles, Int. J. Innov. Res. Sci. Eng. Technol 2 (2013) 5493–5498. http://www.ijirset.com/upload/april/42_Application.pdf.
[6] N. Reddy, Y. Yang, Structure and properties of chicken feather barbs as natural protein fibers, J. Polym. Environ. 15 (2007) 81–87.
[7] L.N. Jones, D. E Riven, D.J. Tucker, Handbook of Fiber Chemistry, Marcel Dekker Inc., New York, 1998.
[8] J.R. Barone, W.F. Schmidt, Polyethylene reinforced with keratin fibres obtained from chicken feathers, Compos. Sci. Technol. 65 (2005) 173–181.
[9] R. Lederer, Integument, feathers, and molt, ornithology: the science of birds, 2005.
[10] M.E. Pahua-Ramos, D.J. Hernández-Melchor, B. Camacho-Pérez, M. Quezada-Cruz, Degradation of chicken feathers: a review, BioTechnol.: Indian J. For. 13 (2017) 153.
[11] R. Dullaart, J. Mousquès, Keratin: Structure, Properties, and Application 164, Nova Science Publishers, Hauppauge, New York, 2012.
[12] J.W. Kock, Physical and Mechanical Properties Chicken Feather Materials, Master of Science Thesis, Georgia Institute of Technology, May 2006.
[13] G. Bansal, V.K. Singh, Review on chicken feather fiber (CFF) a livestock waste in composite material development, Int. J. Waste Resour. 6 (2016) 1–4.

[14] B. Griffith, U.S. Patent application No. 101008. https://patents.justia.com/inventor/barry-allen-griffith, 2001.
[15] C.G. Flores-Hernandez, A. Colin-Cruz, C. Velasco-Santos, V.M. Castaño, J.L. Rivera-Armenta, A. Almendarez-Camarillo, P.E. Garcia-Cassilas, A.L. Martinez-Hernandez, All green composites from fully renewable biopolymers: chitosan-starch reinforced with keratin from feathers, Polym 6 (2014) 686–705.
[16] I.O. Oladele, J.A. Omotoyimbo, S.H. Ayemidejor, Mechanical properties of chicken feather and cow hair fibre reinforced high density polyethylene composites, Int. J. Sci. Technol. 3 (2014) 66–72.
[17] K. Wrześniewska-Tosik, S. Zajchowski, A. Bryśkiewicz, J. Ryszkowska, Feathers as a flame-retardant in elastic polyurethane foam, Fibres Text. East. Eur. 103 (2014) 119–128.
[18] I. Aranberri, S.Montes, I. Azcune, A. Rekonde, H-J Grande, Fully biodegradable biocomposites with high chicken feather content, Polym 9 (2017) 593.
[19] X. Chen, S. Wu, M. Yi, J. Ge, Preparation and physicochemical properties of blend films of feather keratin and poly(vinyl alcohol) Compatibilized by tris(hydroxymethyl)aminomethane, Polym. 10 (2018) 1054.
[20] X. Cao, Y. Chen, P. R, A.D. Chang Muir, G. Falk, Starch-based nanocomposites reinforced with flax cellulose nanocrystals, Express Polym. Lett. 2 (2008) (2008) 502–510.
[21] S.Y.Z. Zainuddin, I. Ahmed, H. Kargarzadeh, Preparation and characterization of cassava starch nanocomposite reinforced kenaf, Adv. Mater. Res. 545 (2012) (2012) 348–352.
[22] S. Karimi, A. Dufresne, M. Tahir, A. Karimi, A. Abdulkhani, Biodegradable starch-based composites: effect of micro and Nano reinforcements on composite properties, J. Mater. Sci. 49 (2014) 4513–4521.
[23] A.T. Issa, K.A. Schimmel, M. Worku, A. Shahbazi, S.A. Ibrahim, R. Tahergorabi, Sweet potato starch-based nanocomposites: development, characterization and biodegradability, Starch 70 (2018) (2018) 1700273.
[24] J.J. Van Heemst, E. Zant, G.J. Schennink, J. Rodenburg, T. Rodenburg, Starch-based biodegradable polymer; method of manufacture and articles thereof. PCT, WO 2011/053131. https://patentimages.storage.googleapis.com/45/fc/2a/13fd5a2c254d24/WO2011053131A1.pdf, 2010. (Accessed 4 April 2019).
[25] C. Bastioli, Global status of the production of biobased packaging materials, Starch 53 (2001) 351–355.
[26] D.R. Tapia-Blácido, P.J. do Amaral Sobral, F.C. Menegalli, Optimization of amaranth flour films plasticized with glycerol and sorbitol by multi-response analysis, LWT - Food Sci. Technol. (Lebensmittel-Wissenschaft -Technol.) 44 (2011) 1731–1738.
[27] D. Muscat, B. Adhikari, R.Adhikari, D.S. Chaudhary, Comparative study of film forming behaviour of low and high amylose starches using glycerol and xylitol as plasticizers, J. Food Eng. 109 (2012) 189–201.
[28] K.M. Dang, R. Yoksan, Development of thermoplastic starch blown film by incorporating plasticized chitosan, Carbohydr. Polym. 115 (2015) 575–581.
[29] M.L. Sanyang, S.M. Sapuan, M. Jawaid, M.R. Ishak, J. Sahari, Effect of plasticizer type and concentration on tensile, thermal and barrier properties of biodegradable films based on sugar palm (*Arenga pinnata*), Starch. Polym. 7 (2015) 1106–1124.
[30] A. Aguirre, R. Borneo, A.E. León, Properties of triticale protein films and their relation to plasticizing–antiplasticizing effects of glycerol and sorbitol, Ind. Crop. Prod. 50 (2013) 297–303.
[31] T.J. Gutiérrez, N.J. Morales, E. Pérez, M.S. Tapia, L. Famá, Physico-chemical properties of edible films derived from native and phosphated cush-cush yam and cassava starches, Food Packag, Shelf Life 3 (2015) 1–8.
[32] A.P. Bilck, C.M.O. Müller, J.B. Olivato, S. Mali, M.V.E. Grossmann, F. Yamashita, Using glycerol produced from biodiesel as a plasticizer in extruded in extruded biodegradable films, Polímeros 25 (2015) 33–335.
[33] V.P. Cyras, L.B. Manfredi, T.T. Minh-Tan, A. Vazquez, Physical and mechanical properties of thermoplastic starch/montmorillonitenanocomposite films, Carbohydr. Polym. 73 (2008) 55–63.
[34] K. Majdzadeh-Ardakani, B. Nazari, Improving the mechanical properties of thermoplastic starch/poly(vinyl alcohol)/clay nanocomposites, Compos. Sci. Technol. 70 (2010) 1557–1563.
[35] V.K. Thakur, D. Vennerberg, M.R. Kessler, Green aqueous surface modification of polypropylene for novel polymer nanocomposites, ACS Appl. Mater. Interfaces 6 (2014) 9349–9356.
[36] C.D. Delhom, Development and thermal characterization of cellulose/clay nanocomposites, Eng. Sci. Univer. New Orleans 62 (2009).
[37] J.W. Lee, S.B. Khan, K. Akhtar, K.I. Kim, T.W. Yoo, K.W. Seo, H. Han, A.M. Asiri, Fabrication of composite membrane based on silicotungstic heteropolyacid doped polybenzimidazole for high temperature PEMFC, Int. J. Electrochem. Sci. 7 (2012) 6276–6288.
[38] D. Kim, M. Jang, J. Seo, K.H. Namb, H. Han, S.B. Khan, UV-cured poly (urethane acrylate) composite films containing surface-modified tetrapod ZnO whiskers, Compos. Sci. Technol. 7 (2013) 84–92.
[39] S.B. Khan, J.W. Lee, H.M. Marwani, K. Akhtar, A.M. Asiri, J. Seo, A.A.P. Khan, H. Han, Polybenzimidazole hybrid membranes as a selective adsorbent of mercury, Compos: Part B.56 (2014) 392–396.
[40] M.M. Damien, G. Eric, C. Carine, Properties of nanofillers in polymer, nanocomposites and polymers with analytical methods, John Cuppoletti, IntechOpen (2011).
[41] A.I. Azmi, R.J.T. Lin, D. Bhattacharyya, Experimental study of machinability of GFRP composites by end milling, Mater. Manuf. Process. 27 (2012) 1045–1050.
[42] S.M. Panamoottil, P. Poetschke, R.J.T. Lin, Conductivity of microfibrillar polymer polymer composites with CNT-loaded microfibrils or compatibilizer: a comparative study,, Express Polym. Lett. 7 (2013) 607–620.
[43] R. Onnainty, G. Granero, Chitosan-clays based nanocomposites: promising materials for drug delivery applications, Nanomed. Nanotechnol. J. 1 (2017) 114.
[44] J.B. Weber, P.W. Perry, R.P. Upchurch, The influence of temperature and time on the adsorption of paraquat, diquat, 2,4-D, and prometone by clays, charcoal, and an anion-exchange resin,, Soil Sci. Soc. Am. Proc. 29 (1965) 678–688.
[45] M.K.S. Monteiroa, V.R.L. Oliveirab, F.K.G. Santosb, E.L. Barros Netoa, R.H.L. Leiteb, E.M.M. Arouchab, R.R. Silvaa, K.N.O. Silvaa, Incorporation of bentonite clay in cassava starch films for the reduction of water vapor permeability, Food Res. Int. 105 (2018) 637–644.
[46] S.L. Abdullahi, A.A. Audu, Comparative analysis on chemical composition of bentonite clays obtained from Ashaka and Tango deposits in Gombe State, Nigeria, Chemsearch J. 8 (2017) 35–40.
[47] L. Jinsong, N. Ivars, Physical and Chemical stability of the bentonite buffer, Chem. Eng. Technol. (2008) 1–43.
[48] L. Carlson, Bentonite mineralogy, geological survey of Finland, Finland, http://www.posiva.fi/files/2257/POSIVA-2004-02_Working-report_web.pdf, Jan. 2004.
[49] M. El Miz, H. Akichoh, D. Berraaouan, S. Salhi, A. Tahani, Chemical and physical characterization of Moroccan bentonite taken from Nador (North of Morocco), Am. J. Chem. 7 (2017) 105–112.
[50] Engineering ToolBox, Specific heat of common substances. https://www.engineeringtoolbox.com/specifec-heat-capacity-d_391.html. (Accessed 8 November 2018).
[51] A. Rabl, P. Curtiss, Principles of Load Calculations, CRC Handbook of Mechanical Engineering, second ed., 2005. http://www.cementechnology.ir/Library/CRC%20Mechanical%20Engineering%20Handbook.pdf.
[52] J. Kosny, D.W. Yarbrough, Thermal Bridges in Building Structures, CRC Handbook of Thermal Engineering, second ed., 2017.
[53] A.O. Ayeni, M.O. Daramola, P.T. Sekoai, O. Adeeyo, M.J. Garba, A.A. Awosusi, Statistical modelling and optimization of alkaline peroxide oxidation pretreatment process on rice husk cellulosic biomass to enhance enzymatic convertibility and fermentation to ethanol, Cellulose 25 (2018) 2487–2504.
[54] A.O. Ayeni, M.O. Daramola, O. Taiwo, O.I. Olanrewaju, D.T. Oyekunle, P.T. Sekoai, F.B. Elehinafe, Production of citric acid from the fermentation of pineapple waste by Aspergillus Niger, Open Chem. Eng. J. 13 (2019) 88–96.